

Inelastic dynamic analysis of a prestressed reinforced concrete frame

J.A. Vásquez & J.C. de la Llera

*National Research Center for Integrated Natural Disaster Management CIGIDEN CONICYT/FONDAP, Chile
Pontificia Universidad Católica de Chile, Santiago, Chile*

M. Rendel

Sirve S.A., Santiago, Chile

ABSTRACT: Customary Seismic design assumes a reduced design spectrum with a certain ductility level of the structure. Although proven successful, the design method provides little information about the inelastic behavior of a structure, which is expected to be large in severe earthquakes. This study deals with the inelastic dynamic response analysis of a large prestressed building to be constructed in Chile. Because of regularity of the structure, a 2D reinforced concrete frame was modeled using fiber elements regularized with a modified stress-strain constitutive relationship using the software Opensees. Therefore, damage may occur anywhere along the element characterized by variable reinforcing steel and internal forces. Results of the inelastic analysis show that inelastic deformations localize in a few places around the nodes, but the building is able to withstand a maximum credible earthquake demand without collapse.

1 INTRODUCTION

Current design methods require a linear elastic model of a structure, and though some detailed analyses are encouraged, they are not mandatory. However, more often than not, inelastic analyses are employed to assess the structural performance of a building, partly due to the quick increase in computer capacity. Nowadays it is possible to compute inelastic dynamic response of a structure in reasonable times. However, these inelastic response analyses can still be very time demanding in cases when: (1) the number of degrees of freedom (d.o.f) of the model is large; (2) the type of elements used in the structural modeling; and (3) the smoothness and complexity of the stress-strain constitutive relationships used.

This study evaluates the inelastic performance of a prestressed Reinforced Concrete (RC) frame using Opensees (McKenna et al. 2000). The building is currently in the design stage and it will be constructed during 2016–2017. Since the building is braced in the longitudinal direction, only a single plane was considered in the unbraced direction; the plane is the one with the highest demand according to a linear analysis. For the sake of simplicity, the timber roof is assumed to remain linear elastic, and the RC frame was modeled using inelastic beam and column fiber element models.

Common approaches in modeling RC frames elements are the plastic hinge models (Scott & Fenves 2006), where nonlinearities concentrate at the element edges, and the distributed plasticity models

(Spacone et al. 1996), which allow nonlinearities across the entire element. In both cases, the element response, depends on the length of the plastic hinge and the number of integration points respectively, i.e. the response is not objective. A distributed plasticity model together with a regularization method for getting objective responses were used. Regularization is obtained by modifying the stress-strain constitutive relationships (Coleman & Spacone 2001; Vásquez et al. 2016) of concrete and steel. This regularization allows for localization of the deformations to be anywhere in the element, which implies that the location of the plastic hinges is an output of the analysis. Generally, plastic hinges will form at the edges of the elements; however, if the reinforcing steel varies along the element to minimize costs, and distributed forces exist, it is possible that plastic hinges form in various places. The prestressed beams were included into the structure after loading them with the slabs. This was modeled using an inelastic construction stage and using auxiliary zero-length elements to account for the initial deformation.

The following section presents the model of the structure and Sections 3 and 4 show the material models and the analysis procedure respectively. Results are summarized in Section 5.

2 STRUCTURAL MODEL

Space limitations impede showing all the details present in building plans. Therefore, we have only

selected some important geometric and mechanical characteristics to include in this and next section. The geometry of the 2D structural model is shown in Figure 1, where there are two types of prestressed beams, the BN135 and VI60, and different columns at each axes B, D, E, and F.

Table 1 summarizes the vertical reactions at the ground level of axes B, D, E, and F, and the vibration periods obtained for the first two modes in different structural models; i.e. (1) a 3D linear elastic Sap2000 v18 model; (2) a 2D linear elastic model in Opensees; and (3) a 2D inelastic model using Opensees, after static loads, prestressing, and before any dynamic loads. The 2D model was loaded using tributary areas, which seems appropriate given the small errors in axial loads in columns, which are less than 2.9% between elastic models. The difference of the sum of all vertical reactions among models is just 1.2%. The difference in period for the first mode is relevant; however, since the consideration of reinforcement steel makes the model stiffer, the dynamic response at low amplitudes

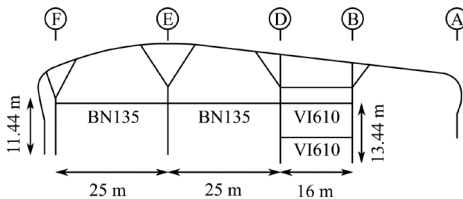


Figure 1. General geometry of the 2D model.

Table 1. Comparison of reactions and periods between 3D and 2D models.

Model	Vertical Reactions				Periods	
	F	E	D	B	1st	2nd
	kN	kN	kN	kN	s	s
3D LE*	1397	3293	2548	1944	0.647	0.374
2D LE*	1373	3384	2556	1940	0.703	0.380
2D NL*	1402	3330	2420	2000	0.652	0.370

*LE refers to linear elastic, and NL to nonlinear.

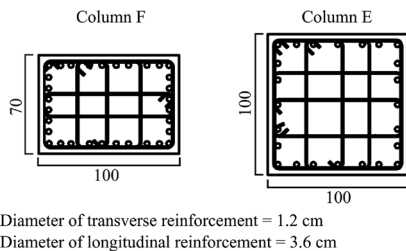
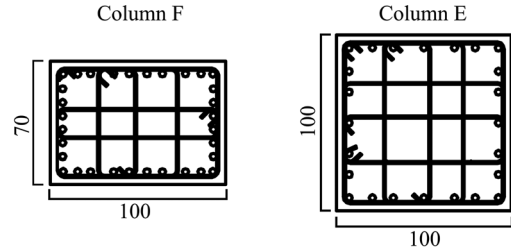


Figure 2. Detailing of active steel bars for beams BN135 and VI60. All dimensions in cm.



Diameter of transverse reinforcement = 1.2 cm
Diameter of longitudinal reinforcement = 3.6 cm

Figure 3. Detailing of columns F and E, all dimensions in cm.

should be very similar to the dynamic behavior of the 3D model used in design.

Shown in Figure 2 is the active steel detailing of beams BN135 and VI610, in which some tendons are unbonded for 2 and 1 meters at the ends of beams BN135 and VI60, respectively. It should be noted that beam VI60 changes the cross section along its length; it is a rectangular section for 1.5 meters at both ends.

Figure 3 shows the reinforcement detailing of columns E and F at the base. The longer dimension of column F is within the plane of the 2D model.

3 MATERIAL MODELS AND REGULARIZATION

The Timber and structural steel used at the roof, and their connections to the RC frame (Fig. 1) were assumed linear elastic, while concrete and steel reinforcing bars in RC sections were modeled using inelastic materials.

3.1 Concrete and steel stress-strain constitutive relationships

Stress-strain relations for concrete and steel are shown in Figure 4. Concrete was modeled using the material Concrete01 of Opensees which neglects tensile strength and is based on the Kent & Park model; Steel02 was used for reinforcement steel, which follows a bilinear backbone curve and includes the Bauschinger effect. This model of steel does not include bar buckling. Although more sophisticated models are available in Opensees, under the proposed regularization scheme explained later in Section 3.2, these models cannot be modified appropriately without intervening the source code, which is deemed unjustified at this stage.

Nominal values were used for concrete and steel properties. Yield stress of steel was 412 MPa at a strain of 0.002, ad a hardening ratio of 1% of the

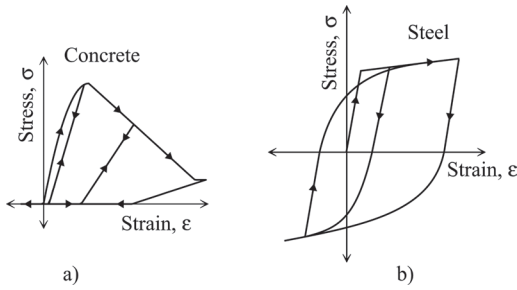


Figure 4. Stress-strain constitutive relations for: (a) concrete, and (b) reinforcement steel—concrete curve shows compression as positive.

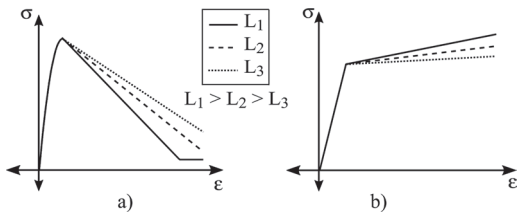


Figure 5. Regularized stress-strain constitutive relationships for: (a) concrete, and (b) reinforcement steel—concrete curve shows compression as positive.

elastic young modulus was considered. The concrete strength used varied according to structural plans; for columns and beams VI60, the strength was 44 MPa, and for beams BN135, the strength was 49 MPa. In all cases the strain at maximum concrete strength was assumed as 0.002.

3.2 Modified stress-strain curves for regularization

Shown in Figure 5 is a schematic representation of the regularization process used, in which the slope was changed according to the length of the integration point of the section. The general idea is that at some point of the element response, deformations will localize in a plastic hinge zone. In distributed plasticity elements, the length of the plastic hinge depends on the number of integration points, since it determines the integration length associated with each section. Consequently, a short length of a plastic hinge will result in high strains, and vice versa, longer lengths will result in lower strains for the same element displacement. Therefore, the regularization consists of giving more deformation capacity to materials located in sections with short integration lengths and the opposite for longer integration lengths. A detailed explanation of this process may be found elsewhere (Coleman & Spacone 2001; Vásquez et al. 2016).

In order to know the different slopes of the descending branches, a fracture length or a fracture energy must be known. For unconfined concrete, the expression for the fracture energy is (Nakamura & Higai 2001):

$$G_{fc} = 8.8 \sqrt{f'_c} \quad (1)$$

Where f'_c is the concrete strength in MPa; and G_{fc} is the compression fracture energy in MPa-mm. For confined concrete, a fracture length of 40 cm associated with a stress-strain Kent & Park relationship was used (Scott et al. 1982). For steel, such energy is not defined, and a fracture length of 30cm had to be assumed, following the recommendations found elsewhere (Vásquez et al. 2016).

4 PRESTRESSED MODELING AND DYNAMIC ANALYSIS

4.1 Prestressed loads

Opensees has not yet implemented a prestressed fiber element. The prestressing was included as follows: (1) model the nonlinear structure with rigid joints; (2) free the rotation degrees of freedom (d.o.f) at the beams ends, and free the axial d.o.f. of one beam end; (3) apply bending moment and axial load due to prestressing at both beam ends simultaneously with all vertical loads present before casting concrete at the joint; (4) add a stiff zero-length element with the Elastic-Perfectly Plastic material of Opensees so that the current local deformations at the freed d.o.f. generate no force in this zero-length elements; and (5) apply roof loads and all additional seismic weight loads.

The prestressed forces are kept constant during the analysis, which is a good approximation if the length of tendons remains approximately the same throughout the analysis. Since prestressed forces, self-weight, and other dead loads produce end rotations of beams about 0.0003 rad, the change in length of tendons is mainly caused by axial deformations in beams since they are long enough to produce non negligible displacements at the beam ends. For the tendons, the Young's modulus is, $E_s = 193191$ MPa, and their areas are 42 cm² and 22.4 cm² for BN135 and VI60 respectively. For concrete $E_c = 27460$ MPa, and the cross sectional area is 5062 cm² and 2880 cm², respectively. The resulting shortening of tendons is in both cases around 5% of the initial tensile displacement at the factory. This means that the original tension force of 195.7 kN was reduced to the final effective force of 186 kN in each cable. Since at beam ends tendons are unbonded and do not transfer loads to concrete, most of the axial loads and bending

moments, though not all, were applied at beam ends. The remaining loads were applied between 1 m and 2 m depending on the structural plans. At the central section, where prestressed loads were fully applied, axial loads were 5872 and 2982 kN for beams BN135 and VI60, respectively. Bending moments result in 4067 and 997 kN-m for these beams, respectively.

Figure 6a shows the exaggerated static deformations before concrete was cast in joints, and Figure 6b when joints are rigid and all seismic weight is applied.

4.2 Dynamic analysis

After applying the prestressing loads and the seismic weight, elastic modes were computed with the actual stiffness at this stage. A Rayleigh damping matrix was assumed with a damping ratio of $\alpha = 3\%$ for periods 0.977s and 0.13s, corresponding to 1.5 and 0.2 times the first mode period of 0.652s. This follows the recommendations found elsewhere (Deierlein et al. 2010). The Newmark method with $\gamma = 1/2$ and $\beta = 1/4$ was used for unconditional stability in the time-domain integration. The default time-domain integration method was Newton-Raphson, and in cases of non-convergence, other algorithms available in Opensees were used, such as the Newton's method with Line Search.

The convergence test was based on the energy increment, and tolerance was set to 10^{-4} tonf-cm which, were the units used in the analysis (or 9.8×10^{-6} kN-m). This tolerance was checked by measuring the external moment at some joints; no error means a zero moment. Analysis results showed that the maximum unbalanced moment reached was 7.2 kN-m with an rms value of 3.4×10^{-5} kN-m at the joint where column E intersects beam BN135.

Finally, the acceleration record selected to validate the model considered a peak ground acceleration (PGA) of 0.43g, consistent with the maximum credible earthquake for the construction site, according to the Chilean seismic provisions (INN 2003).

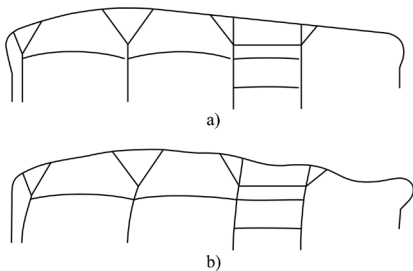


Figure 6. Deformed shape amplified by a factor of 100 for: (a) prestressed and some of the dead loads; and (b) complete seismic weight.

5 RESULTS

Although a large number of responses were obtained, only selected results are presented in this section. Displacements and global responses are presented first, then force-deformation relationships for the sections, and finally stress-strain responses for concrete fibers.

Shown in Figure 7a is the scaled acceleration record used in the analysis. The original record was obtained from a station located in Viña del Mar, Chile, during the 2010, Chile Earthquake in the North-South direction; Figure 7b shows the history of lateral displacement at the level of beam BN135. The remaining plots show the Axial Load Ratio (ALR) history at the top of columns B, D, and E, i.e. the total force on the columns excluding their weights.

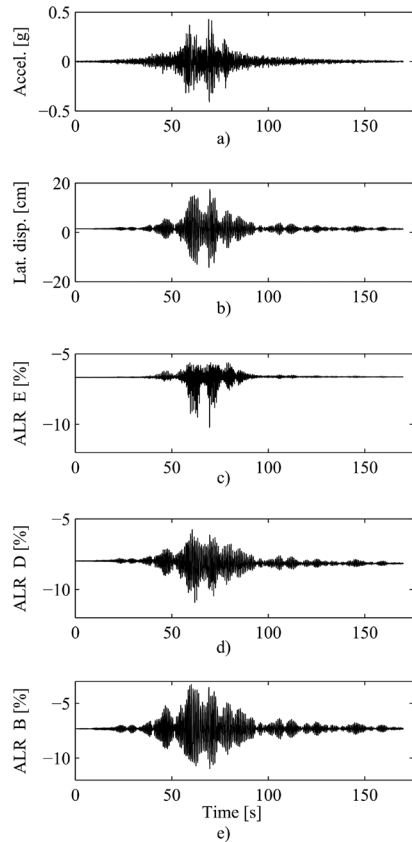


Figure 7. Global structural responses and demand: (a) scaled 2010 Chile, earthquake acceleration record from a station located in Viña del Mar, Chile; b) lateral displacement at beam BN135 level, and Axial Load Ratio (ALR) for (c) column E; (d) column D, and (e) column B.

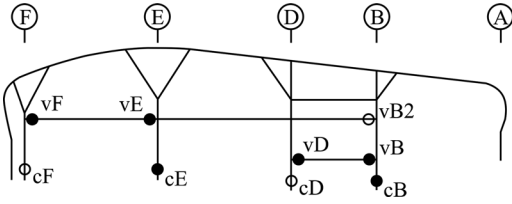


Figure 8. Model with labeled plastic hinges identified after the earthquake analysis; black circle markers indicate that section responses will be shown here.

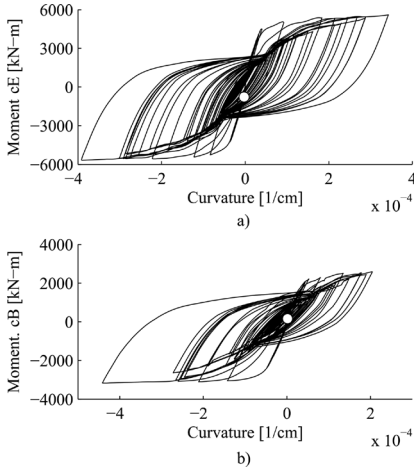


Figure 9. Moment curvature response at bottom hinges in: (a) column E; and (b) column B—white circles mark the initial point of the dynamic analysis.

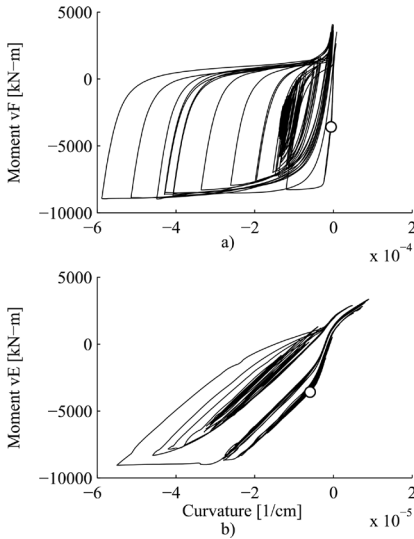


Figure 10. Moment curvature response in beam BN135 in hinges next to: (a) axis F; and (b) axis E.

Figure 8 identifies the location of all plastic hinges with a circle marker, and the filled ones are the selected locations for showing section responses. Note that column hinges are slightly above ground level since in these zones columns widen dramatically, remaining elastic throughout the analysis.

Shown in Figure 9 is the moment-curvature response for hinges cE and cB. Although deforma-

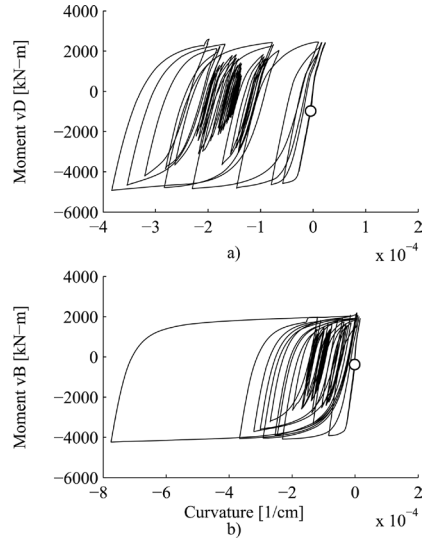


Figure 11. Moment curvature response of hinges in beam VI60 at (a) axis D; and (b) axis B.

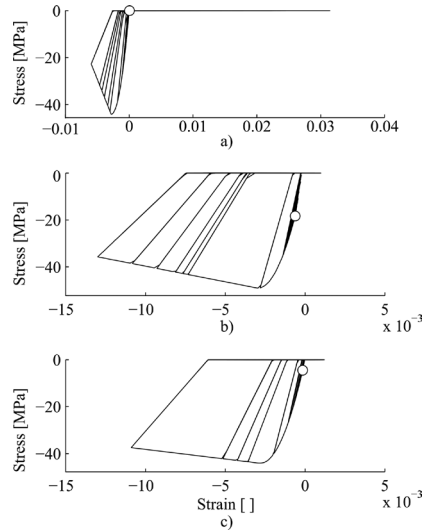


Figure 12. Stress-strain responses of the outermost fiber of concrete cover for hinges: (a) vF; (b) vB; and (c) cE.

tions are not directly comparable between them due to the regularization used, for both cases the ultimate capacity is not reached

Shown in Figure 10 is the moment curvature response at both ends of beam BN135 between axes F and E (Fig. 8). Because in this case both sections have the same length, their results are directly comparable. It is apparent that extreme F has much larger demand than the end next to axis E by a deformation approximately ten times larger. In all cases plastic hinges do not reach their ultimate capacity.

Figure 11 shows the same responses, but this time, for the beam VI60 at the intersection with axes D and B. In this case the curvature demand is similar, though the right hinge vB shows twice the curvature of the left hinge vD. Similar to previous cases, the ultimate capacity is not reached.

From all possible fiber responses, only the resulting stress-strain relations of concrete are shown in Figure 12 for the three cases corresponding to Figures 9a, 10a, and 11b. This enables the reader to do a simple comparison between all curves by watching the stress at the maximum compressive strain in each case. It is clear that cE is the hinge with largest demand, followed by vF, and finally vB.

6 CONCLUSIONS

This paper presented the inelastic model and earthquake response of a 2D RC prestressed frame using the software Opensees. Both, regularization and prestressed forces, were added since they are not directly implemented in the software. Although a single ground motion was used for demonstrative purposes, the following conclusions can be drawn:

1. Although the acceleration record used corresponds to a maximum credible earthquake none of the plastic hinges reached their ultimate capacity.
2. The formation of plastic hinges was very different, and only a dynamic inelastic analysis is capable of showing the differences in demand throughout the structure. Regularization ensures that these demands are not mesh dependent.
3. All columns form plastic hinges and the analysis results show that column E undergoes larger demands, which was indeed a concern at the design stage.

Finally, more complex models could be used to improve the analysis, such as steel with realistic hardening and buckling behavior, and prestressed forces coming from cable deformations instead of constant external forces. A next step is to do an incremental dynamic analysis, and compute the response of the structure under different excitation levels causing different damage states in the building.

ACKNOWLEDGEMENTS

This research has been sponsored by the National Research Center for Integrated Natural Disaster Management CONICYT/FONDAP/15110017 and by Fondecyt grant #1141187. Also, authors are grateful to SIRVE S.A. for providing the building design information.

REFERENCES

- Coleman, J. & Spacone, E. 2001. Localization issues in nonlinear frame elements. *Modeling of inelastic behavior of RC structures under seismic loads*, 403–419.
- Deierlein, G.G., Reinhorn, A.M. & Willford, M.R. 2010. *Nonlinear Structural Analysis for Seismic Design: A Guide for Practicing Engineers*, NIST, National Institute of Standards and Technology, California.
- INN. 2003. Análisis y diseño de edificios con aislación sísmica, Santiago, Chile
- McKenna, F., Fenves, G. & Scott, M. 2000. Open system for earthquake engineering simulation. *University of California, Berkeley, CA*.
- Nakamura, H. & Higai, T. 2001. Compressive fracture energy and fracture zone length of concrete. *Modeling of inelastic behavior of RC structures under seismic loads*, 471–487.
- Scott, B.D., Park, R. & Priestley, M.J.N., 1982, January. Stress-strain behavior of concrete confined by overlapping hoops at low and high strain rates. In *Journal Proceedings* 79(1): 13–27).
- Scott, M.H. & Fenves, G.L. 2006. Plastic hinge integration methods for force-based beam–column elements. *Journal of Structural Engineering* 132(2): 244–252.
- Spacone, E., Filippou, F.C. & Taucer, F.F. 1996. Fibre beam-column model for non-linear analysis of R/C frames: Part I. Formulation. *Earthquake engineering and structural dynamics*, 25(7):711–726.
- Vásquez, J.A., de la Llera, J.C. & Hube, M.A. 2016. A regularized fiber element model for reinforced concrete shear walls. *Earthquake Engineering & Structural Dynamics*.